The Domain Chaos Puzzle and the Moments of the Swift-Hohenberg Structure Factor

Nathan Becker* and Guenter Ahlers†
Department of Physics and iQUEST, University of California, Santa Barbara, California 93106
(Dated: May 23, 2019)

Integration of the Swift-Hohenberg (SH) structure factor (SF) provided analytic results for the total power P, the first moment $\overline{k}$, and the variance σ^2. Comparison of $\sigma = 1/\overline{\xi}$ with the half-width $1/\xi$ shows that $\overline{\xi} \sim \sqrt{\xi}$. This may explain previous experimental results for domain chaos in Rayleigh-Bénard convection with rotation that indicated $\overline{\xi} \sim \varepsilon^{-\nu_{eff}}$ (ε is the distance above threshold) with $\nu_{eff} \simeq 1/4$ in apparent disagreement with the theoretical prediction of $\xi \sim \varepsilon^{-\nu}$ with $\nu = 1/2$. Fitting the SH SF to new data yielded $\nu \simeq 0.41$, considerably closer to the prediction.

Spatially extended nonlinear non-equilibrium systems continue to be of great interest because they yield qualitatively different phenomena that do not occur in linear systems [1]. One of these phenomena is spatio-temporal chaos. The examples of spatio-temporal chaos found in Rayleigh-Bénard convection (RBC) lend themselves to particularly detailed experimental study under exceptionally well controlled external conditions [2]. RBC occurs in a thin horizontal layer of fluid with thickness d heated from below when the temperature difference ΔT exceeds a critical value ΔT_c.

Particularly noteworthy is the state that occurs in RBC when the fluid layer of density ρ and shear viscosity η is rotated about a vertical axis with angular frequency ω. When the dimensionless frequency $\Omega \equiv \omega d^2 \rho/\eta$ exceeds a critical value, then the pattern immediately above onset consists of disordered domains of convection rolls known as domain chaos. This is illustrated in Fig. 1a. Within each domain the roll orientation is more or less uniform; but different domains have different orientations [3, 4, 5]. The domains are unstable and undergo a persistent but irregular dynamics. In this case, the time-averaged mean-square velocities and temperature deviations from the conduction state grow continuously from zero as ΔT_c is exceeded, i.e. the bifurcation is supercritical.

Chaos immediately above a supercritical bifurcation offers a unique opportunity for theoretical study because weakly-nonlinear theories are expected to be applicable. These theories, in the form of Ginzburg-Landau (GL) or Swift-Hohenberg (SH) equations, by virtue of their general structure and from their numerical solutions, predict that the inverse half-width at half-height ξ of the structure factor (SF, the square of the modulus of the Fourier transform of the patern) should vary as $\varepsilon^{-\nu}$ with $\nu = 1/2$ as $\varepsilon \equiv \Delta T/\Delta T_c - 1$ vanishes [6, 7, 8], and that it is the only length scale in the problem. Thus it was particularly disappointing that measurements for domain chaos seemed to disagree with this expectation [4]. Determinations of a correlation length $\bar{\xi}$ based on the variance of the SF found $\bar{\xi} \propto \varepsilon^{-\nu_{eff}}$ with $\nu_{eff} \simeq 1/4$ rather than 1/2.

Several possible explanations of the apparent disagreement with theory were explored by various authors. Hu et al. proposed that defects and fronts injected by the side wall into the bulk may play an important role [5]. Laveder et al. demonstrated that additive white noise intended to mimic the effect of wall defects decreases ν to the value of ν_{eff} measured experimentally provided that the noise level is sufficiently large [9]. Recent unpublished experiments in our group using a sample with a radially ramped spacing [10] render the side-wall-injected defect idea an unlikely explanation. On the basis of numerical simulation using a SH equation Cross et al. proposed that the finite size of the experimental convection cell decreases the effective value of ν [11]. Experiments with samples of different lateral extent are not yet sufficient to support this idea.

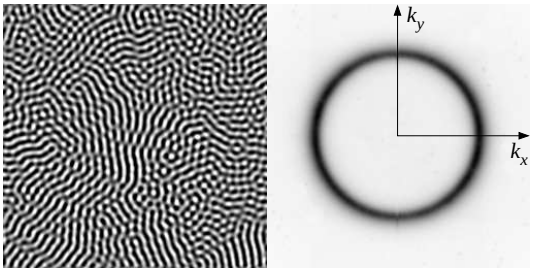

FIG. 1: Left: shadowgraph image of size $57d \times 57d$ for $\Omega = 21.7$ and $\varepsilon = 0.06$. Right: the average structure factor $S(k, \theta)$ of 4096 images like the one on the left.

In the present paper we offer an alternative explanation of the apparent conflict between theory and experiment. Experimental determinations of a characteristic length scale $\bar{\xi}$ usually are based on numerical estimates of the variance σ^2 (see Eq. 6 below) of the SF, with $\bar{\xi}^2 = \sigma^{-2}$ [4, 12]. We show that $\bar{\xi}$ does not have the same ε-dependence as the inverse half-width at half height ξ. We demonstrate this analytically for the SF of the linear SH equation

$$S(k) = \frac{4k_0^2 B}{\xi^2 \left(k^2 - k_0^2\right)^2 + 4k_0^2} \tag{1}$$

where we find $\bar{\xi} \sim \sqrt{\xi}$ for large ξ. This result is obtained also for instance for a Lorentzian SF corresponding to a GL equation. However, for a Gaussian distribution one finds $\bar{\xi} \sim \xi$. Similarly, $\bar{\xi} \sim \xi$ was found when $S(k)$ was

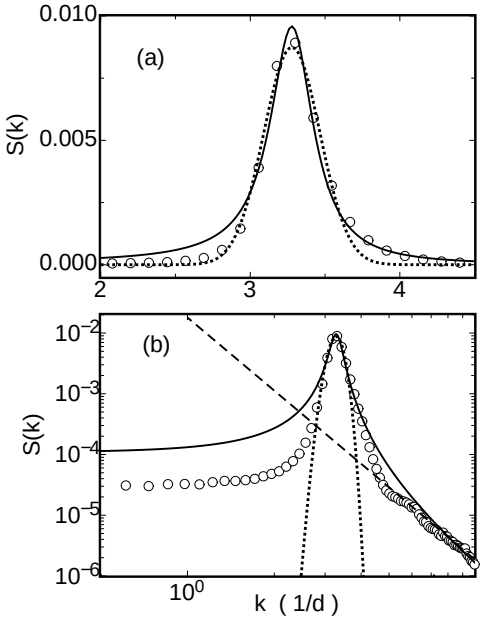

FIG. 2: The average structure factor $S(k)$ of 128 images for $\Omega = 16.25$ and $\varepsilon = 0.136$. (a): $S(k)$ on linear scales. (b): $S(k)$ on logarithmic scales. Solid lines: fit of Eq. 1 to the data. Dotted lines: fit of a Gaussian function to the data. Dashed line in (b): the powerlaw $S(k) \sim k^{-4}$.

set equal to the *square* of the rhs of Eq. 1, as was done by some authors when fitting to numerical results for $S(k)$ in order to estimate a half width of the distribution [13].

We also present new experimental data for domain chaos and show that fits of Eq. 1 to the experimental SF yield results for ξ that have an effective exponent ν in much better agreement with the prediction $\nu = 1/2$ than the result $\nu_{eff} \simeq 1/4$ obtained from the variance of the experimental $S(k)$.

The exact form of the SF for domain chaos is not known. There are two arguments in favor of using Eq. 1 as a model for the SF of domain chaos. First, it is an excellent approximation to the SF of the linearized full equations of motion (the Boussinesq equations) in the presence of additive noise for RBC below onset [14]. Perhaps more importantly, its large-k dependence on k^{-4} agrees well with experimental results for the nonlinear state above onset. The Lorentzian and squared SH equations yield $S(k) \sim k^{-2}$ and $S(k) \sim k^{-8}$ respectively at large k and in this respect disagree with experiment.

Figure 1b shows an average $S(k,\theta)$ of the structure factors of 4096 images such as the one in Fig. 1a. One sees that it is rotationally invariant, reflecting the symmetry of the Rayleigh-Bénard system. Thus we consider an azimuthal average $S(k)$ of $S(k,\theta)$. In Fig. 2a we show a typical experimental example. The solid line in that figure corresponds to a fit of Eq. 1 to the data, with B, k_0, and ξ least-squares adjusted. One sees that the equation fits quite well except at small k where it is too large. We note especially that it fits well near the half-height $S(k) = B/2$ where the width of $S(k)$ determines ξ.

In Fig. 2b the same data are shown on double logarithmic scales. The difference between the data and Eq. 1 at small k is seen more clearly. This part contributes relatively little to the moments. At large k both data and function vary in proportion to k^{-4}. Below onset the structure factor for fluctuations derived from the Boussinesq equations also has this k-dependence. In that case it originates from the coupling via external noise of two modes (temperature and velocity), each of which by itself would have a k^{-2} dependence typical of diffusion [14]. Details of mode interaction are not understood for the nonlinear chaotic state above onset. Thus it is interesting to note from experiment that it produces the same k-dependence of $S(k)$ at large k. For the purpose at hand we note that the large-k part of $S(k)$ contributes more to the moments, and it is reassuring that Eq. 1 and the data agree quite well in this range.

Returning to Eq. 1, we note that the position of the peak of $S(k)$ is at k_0 and $S(k_0) = B$. The correlation length ξ approaches the reciprocal of the half-width when it becomes large. The total power $P = 2\pi \int_0^\infty S(k)\, k dk$ is

$$P = \frac{2\pi k_0 B}{\xi}\left[\frac{\pi}{2} - \tan^{-1}\left(-\frac{\xi k_0}{2}\right)\right] . \qquad (2)$$

An expansion for large ξ gives

$$P = \frac{2\pi^2 k_0 B}{\xi}\left[1 - \frac{2}{\pi\xi k_0} + \mathcal{O}\left(\frac{1}{\xi^3}\right)\right] . \qquad (3)$$

At small ε one expects $\xi \sim \varepsilon^{-\nu}$ with $\nu = 1/2$. One also expects the total power to vanish at onset in proportion to ε. Thus, if Eq. 1 gives the shape of $S(k)$ correctly, one has $P \sim \varepsilon^{\nu+\beta}$ with $\nu + \beta = 1$, and $B \sim \varepsilon^{\beta}$ with $\beta = 1/2$. The mean wave number is equal to the first moment

$$\begin{aligned} \overline{k} &= \frac{2\pi \int_0^\infty S(k)\, k^2 dk}{P} \qquad (4) \\ &= k_0 \frac{\frac{2}{\xi k_0}\sin\left[\frac{1}{2}\tan^{-1}\left(\frac{2}{\xi k_0}\right)\right] + \cos\left[\frac{1}{2}\tan^{-1}\left(\frac{2}{\xi k_0}\right)\right]}{\left(1+\frac{4}{\xi^2 k_0^2}\right)^{1/4}\left[\frac{1}{2} - \frac{1}{\pi}\tan^{-1}\left(-\frac{\xi k_0}{2}\right)\right]} . \end{aligned}$$

It is only approximately equal to the position of the peak k_0 because the distribution is skewed. For large ξ one has

$$\overline{k} = k_0\left[1 + \frac{2}{\pi\xi k_0} + \mathcal{O}\left(\frac{1}{\xi^2}\right)\right] . \qquad (5)$$

The second moment is not finite when the limits of the integral are allowed to range from 0 to ∞ because of a logarithmic divergence at large k. Nevertheless, the use of a finite cutoff k_C permits the calculation of the relation between ξ and the variance

$$\sigma^2 = \frac{2\pi}{P}\int_0^{k_C} S(k)\, k^3 dk - \overline{k}^2 . \qquad (6)$$

The variance is

$$\sigma^2 = \frac{k_0^2\left\{\tan^{-1}\left(\frac{\xi}{2k_0}\left[k_C^2-k_0^2\right]\right)+\tan^{-1}\left(\frac{\xi k_0}{2}\right)\right\}+\frac{k_0}{\xi}\ln\left(\frac{4k_0^2+\xi^2\left[k_C^2-k_0^2\right]^2}{4k_0^2+\xi^2k_0^4}\right)}{\tan^{-1}\left(\frac{\xi k_C^2}{2k_0}-\frac{\xi k_0}{2}\right)-\tan^{-1}\left(-\frac{\xi k_0}{2}\right)}-\overline{k}^2 \tag{7}$$

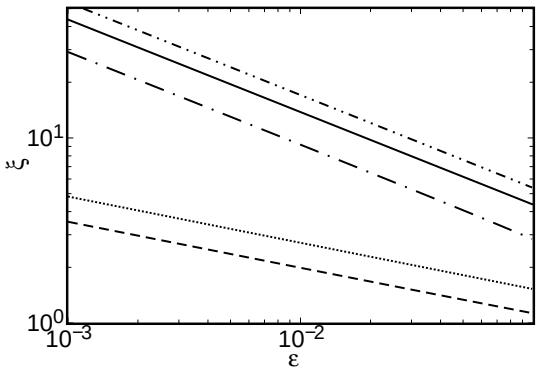

FIG. 3: Correlation lengths ξ and $\bar{\xi}$ as a function of ε. The solid line $\xi = 1.34/\sqrt{\varepsilon}$ roughly passes through the data in Fig. 4 near $\varepsilon = 0.03$ and was used to obtain the other lines. Dashed line: exact result for $\bar{\xi} = 1/\sigma$ (σ^2 from Eq. 7) with $k_C = 14$. Dotted line: small-ε approximation for $\bar{\xi}$ (σ^2 from Eq. 8) with $k_C = 14$. Dash-dotted and dash-double-dotted lines: $\bar{\xi}$ based on Eq. 7 with integration cutoffs given by Eq. 9 and $\gamma = 0.05$ and 0.25 respectively.

For a systematic evaluation of σ^2 the mean wave number $\bar{k}$ should be evaluated using the same cutoff k_C. The exact analytic expression for $\bar{k}$ with a finite cutoff is complicated and will not be reproduced here. For large ξ (but with $\overline{k}^2$ evaluated without a cutoff) one has

$$\sigma^2 \simeq \frac{1}{\xi}\left[\frac{k_0}{\pi}\ln\left(\frac{\left[k_C^2-k_0^2\right]^2}{k_0^4}\right)\frac{4k_0}{\pi}\right]+\mathcal{O}\left(\frac{1}{\xi^2}\right) \tag{8}$$

In this approximation we see that the cutoff affects the amplitude of σ^2 but not its ξ-dependence. As mentioned earlier, some previous experimental and numerical work used $\overline{\xi} \equiv 1/\sigma$. Equation 8 implies that $\overline{\xi} \sim \sqrt{\xi}$. Assuming that $\xi \sim \varepsilon^{-1/2}$ this implies that $\overline{\xi} \sim \varepsilon^{-1/4}$, similar to what had been found in early experiments [4].

We note that for the squared SH equation (i.e. $S(k)$ set equal to the square of the rhs of Eq. 1) one obtains $\sigma^2 = \xi^{-2}[1 - 8/(3\pi k_0\xi) + \mathcal{O}(\xi^{-2})]$, i.e. $\bar{\xi} \sim \xi$, and a half width at half height that approaches $\sqrt{\sqrt{2}-1}/\xi$ for large ξ.

Figure 3 shows the implications of Eqs. 7 and 8 for the example $\xi = 1.34\varepsilon^{-1/2}$ (solid line) chosen so that it approximately passes through the experimental data in Fig. 4 near $\varepsilon = 0.03$. The approximate result Eq. 8 (dotted line) has a slope of $-1/4$. The exact result for $\overline{\xi}$ (dashed line) obtained with $k_C = 14$ deviates only very little from the $\varepsilon^{-1/4}$ powerlaw. The choice of k_C roughly coincides with the maximum experimentally accessible value of k_C for the present apparatus.

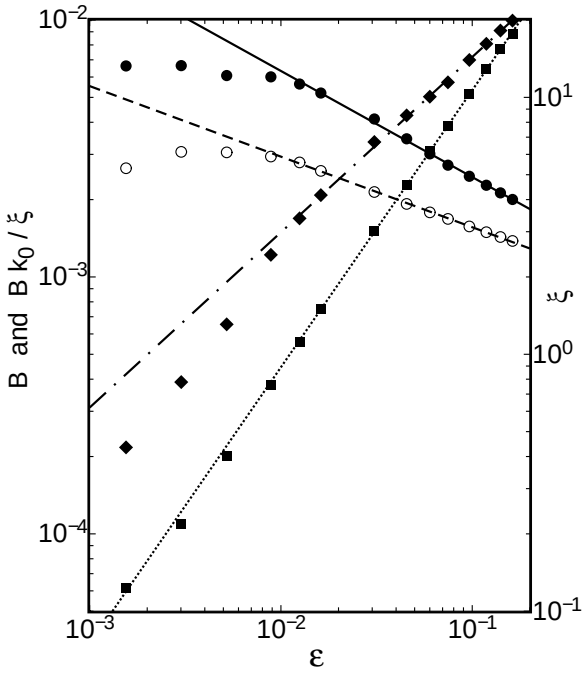

FIG. 4: Parameters derived from the structure factors at $\Omega = 21.7$. Open circles: $\bar{\xi}$ (right ordinate) obtained from the moments of $S(k)$ calculated between the limits $k_- = 1.6$ and $k_+ = 5.6$. The solid symbols are derived from fits of Eq. 1 to the data for $S(k)$. Circles: ξ (right ordinate). Diamonds: B (left ordinate). Squares: Bk_0/ξ (left ordinate). The lines are fits of power laws to the data for $\varepsilon \geq 0.01$. The fits to ξ, $\bar{\xi}$, B, and Bk_0/ξ gave exponent values $\nu = 0.413$, $\bar{\nu} = 0.275$, $\beta = 0.682$, and $\beta + \nu = 1.078$ respectively.

In the analysis of actual experimental data a number of practical considerations come into play and lead to uncertainties of the derived exponents. For the present work we determined a background for $S(k)$ below onset, corresponding primarily to experimental noise contributions, and subtracted it from $S(k)$ at $\varepsilon > 0$. When this subtraction is not carried out, it leads to a reduction of $\bar{\xi}$

that is relatively large at small ε, where $S(k)$ is relatively small, thus yielding a value of ν_{eff} that is too small. Another practical issue is the choice of limits used for the numerical sums over the data for $S(k)$ that yield the variance. In some previous experimental measurements, the limits $k_\pm$ were chosen such that $S(k_\pm) = \gamma S(k_0)$ where $\gamma = 0.15$ [4, 15]. Applying this method to Eq. 1 for $S(k)$ reveals that $k_\pm$ is ξ-dependent:

$$k_\pm = \sqrt{k_0^2 \pm \frac{2k_0}{\xi}\sqrt{\frac{1-\gamma}{\gamma}}}\ . \qquad (9)$$

The dash-dotted and dash-double-dotted lines in Fig. 3 show numerically that Eq. 9 yields $\overline{\xi} \propto \xi$. This is particularly problematic because it implies that ξ-dependent limits artificially modify the ε dependence of the variance. Although not shown in the figure, the choice of constant values for $k_\pm$, independent of ξ, gives $\overline{\xi} \propto \sqrt{\xi}$.

By using various integration limits and treatments of experimental background we were able to produce a range of values for ν_{eff}, but ν was relatively immune to these variations in the data analysis. In view of this, we prefer to determine the width ξ of $S(k)$ from fits of the SH form Eq. 1 to the data. We found that the result for ξ is not very sensitive to the form of the equation used in the fits. A Lorentzian yielded nearly identical values for the half width. When a Gaussian function $\exp[-(\ln 2)(k-k_0)^2\xi^2]$ (as illustrated in Fig. 2) or a squared SH SF were used, the results for ξ were slightly smaller but yielded almost the same value for ν.

Figure 4 shows new results for ξ (solid circles) derived from fits of Eq. 1 to $S(k)$ for data taken at $\Omega = 21.7$ in an apparatus described before [16]. The sample was compressed SF_6 gas at a pressure of 20.00 bars and mean temperature of 38.00°C where the Prandtl number $\eta/(\rho\kappa)$ (κ is the thermal diffusivity) was 0.87. The aspect ratio $\Gamma \equiv D/2d$ (D is the sample diameter) was 61.5. For $\varepsilon \geq 0.01$ a power-law fit to ξ yielded $\nu \simeq 0.41$, much closer to the theoretical prediction 1/2 than previously reported results for ν_{eff} [4, 5]. Previous measurements [4, 5] were all for $\epsilon > 0.01$. We do not know the reason for the rounding of the present data at smaller ε. Contributing factors could include finite image-size effects that come into play when the correlation length is large, finite sample-size effects [11], small inhomogeneities of the sample spacing, and centrifugal-force effects.

Numerical integration of the data over the range $1.6 < k < 5.6$ yielded the open circles in the figure for $\overline{\xi}$. For $\varepsilon \geq 0.01$ those results yielded $\nu_{eff} = 0.28$, close to the value of 1/4 predicted by Eq. 8 and the previously reported experimental result [4].

In Fig. 4 we show also results for B (solid diamonds) and for Bk_0/ξ (solid squares). For $\varepsilon > 0.01$ the data for B yield an exponent $\beta = 0.68$, somewhat larger than the expected value 1/2. It is possible that this difference reflects a difference in the shapes of the actual and the SH structure factor. As for ξ, the data at small ε deviate from the power law. Interestingly, the results for Bk_0/ξ follow a power law over the entire range of the data, to ε-values as small as 10^{-3}. The dotted line in the figure corresponds to an exponent of 1.08, to be compared with the expected value $\beta + \nu = 1$.

Although the new result for ν still differs somewhat from the theoretical value, it is not so far away from the theory that one can argue for a genuine disagreement. Several factors could possibly account for the remaining difference. These include the precise choice for ΔT_c and possible finite sample-size effects as suggested by Cross *et al.* [11]. In addition, the rounding at small ε so far has prevented us from measuring an unencumbered ξ for $\varepsilon < 0.01$. In the accessible ε range confluent corrections to the leading power law may influence the experimental value of ν.

This work was supported by the National Science Foundation through Grant DMR02-43336.

* Electronic address: nbecker@physics.ucsb.edu
† Electronic address: guenter@physics.ucsb.edu

[1] See, for instance, M.C. Cross and P.C. Hohenberg, Rev. Mod. Phys. **65**, 851 (1993).
[2] For a review, see for instance E. Bodenschatz, W. Pesch, and G. Ahlers, Annu. Rev. Fluid Mech. **32**, 709 (2000).
[3] G. Küppers and D. Lortz, J. Fluid Mech. **35**, 609 (1969); G. Küppers, Phys. Lett. **32A**, 7 (1970); R.M. Clever and F.H. Busse, J. Fluid Mech. **94**, 609 (1979); K.E. Heikes and F.H. Busse, Ann. N.Y. Acad. Sci. **357**, 28 (1980); F.H. Busse and K.E. Heikes, Science **208**, 173 (1980).
[4] Y.-C. Hu, R. Ecke, and G. Ahlers, Phys. Rev. Lett. **74**, 5040 (1995); Phys. Rev. E **55**, 6928 (1997).
[5] Y. Hu, W. Pesch, G. Ahlers, and R.E. Ecke, Phys. Rev. E **58**, 5821(1998).
[6] J.M. Rodriguez, C. Perez-Garcia, M. Bestehorn, M. Fantz, and R. Friedrich, Phys. Rev. A **46**, 4729 (1992); M. Fantz, R. Friedrich, M. Bestehorn, and H. Haken, Physica D **61**, 147 (1992); M. Neufeld, R. Friedrich, and H. Haken, Z. Phys. B **92**, 243 (1993).
[7] Y. Tu and M. Cross, Phys. Rev. Lett. **69**, 2515 (1992); M. Cross, D. Meiron, and Y. Tu, Chaos **4**, 607 (1994).
[8] Y. Ponty, T. Passot, and P. Sulem, Phys. Rev. Lett. **79**, 71 (1997); Phys. Rev. E **56**, 4162 (1997).
[9] D. Laveder, T. Passot, Y. Ponty, and P. L. Sulem, Phys. Rev. E **59**, R4745 (1999).
[10] K.M.S. Bajaj, N. Mukolobwiez, N. Currier, and G. Ahlers, Phys. Rev. Lett. **83**, 5282 (1999).
[11] M. C. Cross, M. Louie, and D. Meiron, Phys. Rev. E63, 45201 (2001).
[12] S. W. Morris, E. Bodenschatz, D. S. Cannell, and G. Ahlers, Phys. Rev. Lett. **71**, 2026 (1993).
[13] M.C. Cross and D.I. Meiron, Phys. Rev. Lett. **75**, 2152 (1995); Q. Hou, S. Sasa, and N. Goldenfeld, Physica A **239**, 219 (1997).
[14] J. M. Ortiz de Zárate and J. V. Sengers, Phys. Rev. E **66**, 036305 (2002).

[15] Y.-C. Hu, Ph.D. Thesis, University of California at Santa Barbara, 1995 (unpublished).
[16] J.R. deBruyn, E. Bodenschatz, S. Morris, S. Trainoff, Y.-C. Hu, D.S. Cannell, and G. Ahlers, Rev. Sci. Instrum. **67**, 2043 (1996).